Supplementary Information of

Optimizing the piezocatalytic hydrogen production activity of metal-organic frameworks through precise defect engineering

Author Information

Affiliations

[a]School of Science, Harbin Institute of Technology, Shenzhen 518055, PR China

[b]School of Ecology and Environment, Harbin Institute of Technology, Shenzhen 518055, PR China

Bing Wang[a#], Zhen Sun[b#], Jiahui Chen[a], Jiayin Ye[a], Abhinandan Kumar[a], Peng Ren[a]*, Guan Zhang[b]*, Jin Zhang[a]*

[#]Contributed equally.

*Corresponding author. E-mail address: renpeng@hit.edu.cn (P. Ren), zhangguan@hit.edu.cn (G. Zhang), jinzhang@hit.edu.cn (J. Zhang)

1. Number of missing BDC linker characterization by TGA

Here, we define *x* as the number of missing BDC linkers in the material. In this study, we define *m* as the ratio of the mass at 450°C to the final mass at 600°C, with subscripts indicating different temperatures. The number of missing BDC linkers (*x*) in the structure can be determined using the following equation[S1]:

$$m_{600} = MW_{HfO_2} \cdot n_{HfO_2} \#\ (S1)$$

$$n_{MOF} = \frac{n_{HfO_2}}{6} = \frac{m_{600}}{6 \cdot MW_{HfO_2}} = \frac{100}{6 \cdot MW_{HfO_2}} \#(S2)$$

$$m_{450} = MW_{MOF_{450}} \cdot n_{MOF} \#(S3)$$

$$MW_{MOF_{450}} = \frac{6 \cdot m_{450} \cdot MW_{HfO_2}}{100} = 12.63 \cdot m_{450} \#(S4)$$

$$MW_{MOF_{450}} = 6 \cdot MW_{Hf} + (6 + x)\, MW_O + (6 - x) MW_{BDC^{2-}} \#(S5)$$

$$x = \frac{MW_{\mathrm{MOF}_{450}} - 6\left(MW_{\mathrm{Hf}} + MW_{\mathrm{O}} + MW_{\mathrm{BDC}^{2-}}\right)}{MW_{\mathrm{O}} - MW_{\mathrm{BDC}^{2-}}} = \frac{2151.71 - 12.63 \cdot m_{450}}{148.13} \#(\mathrm{S6})$$

2. Defect concentration calculations of UiO-66 models in MD simulations

To quantify the defect concentration of UiO-66 models considered in MD simulations, we adopted the same definition as commonly used in ^{1}H-NMR experimental analysis, by comparing the relative amounts of terephthalate linkers (BDC) and formate groups ($HCOO^-$). In the *fcu* configuration, each Hf node is fully coordinated by 6 BDC linkers and contains no formate group. In the *reo* configuration, missing-linker defects reduce the coordination to 4 BDC linkers per Hf node, while the remaining coordination sites are compensated by 4 $HCOO^-$ groups.[S2]

Thus, as for a simulation supercell consisting of N units, where n units adopt the *reo* configuration and the remaining ($N-n$) units adopt the *fcu* configuration, the corresponding total numbers of BDC and HCOO groups, namely n_{BDC} and n_{HCOO} can be calculated as:

$$n\mathrm{BDC} = 6(N - n) + 4n \#(\mathrm{S7})$$

$$n\mathrm{HCOO} = 4n \#(\mathrm{S8})$$

The defect concentration c can be correspondingly defined as follows:

$$c = \frac{n\mathrm{HCOO}}{n\mathrm{BDC}} \#(\mathrm{S9})$$

Based on Equation S9, the defect concentration of UiO-66 models with different numbers of the defective *reo* units ranging from 0 to 10 varies from 0% to 28% correspondingly.

3. The carrier concentration (N_{D}) and conduction band (C_{B}) position calculated from the Mott-Schottky measurements

The space-charge capacitance C of the electrode semiconductor interface obeys:[S3, 4]

$$\frac{1}{C^2} = \left(\frac{2}{\varepsilon_0 \varepsilon_{\mathrm{r}} A^2 e N_{\mathrm{D}}}\right)\left(V - V_{\mathrm{FB},SHE} - \frac{k_{\mathrm{B}}T}{e}\right) \#(\mathrm{S10})$$

Here, C is the interfacial capacitance and A is the geometric electrode area, respectively. N_{D} is the number of

carrier concentration, V is the applied voltage, k_B is Boltzmann's constant, T the absolute temperature, and e is the electronic charge, ε_r is relative dielectric constant, ε_0 the vacuum dielectric constant. At 298 K, $K_BT/e \approx 0.0257$ V can be ignored at room temperature.

The slope of the linear fitting to the second half of the $1/C^2$ versus V plot is denoted as S. Therefore, N_D can be estimated as:

$$N_D = \frac{2}{\varepsilon_r \varepsilon_0 e S A^2} \#(S11)$$

The flat-band potential is obtained from the x-intercept of the linear fit:

$$V_{FB,SHE} = V_{intercept} - k_BT/e \#(S12)$$

For an n-type semiconductor, the conduction band edge is estimated from the flat-band potential with a small band-bending correction $\Delta\Phi$, which was taken as 0.2 V here.

$$C_{B,SHE} = V_{FB,SHE} + \Delta E - \Delta\Phi \#(S13)$$

The reference electrode ΔE was +0.197V for Ag/AgCl (saturated KCl, vs SHE at 25 °C). Accordingly, the valence band edge was determined as follows:

$$V_{B,SHE} = C_{B,SHE} + E_g \#(S14)$$

where E_g is obtained from the Tauc plot (Fig. S15).

4. Supplementary figures and tables

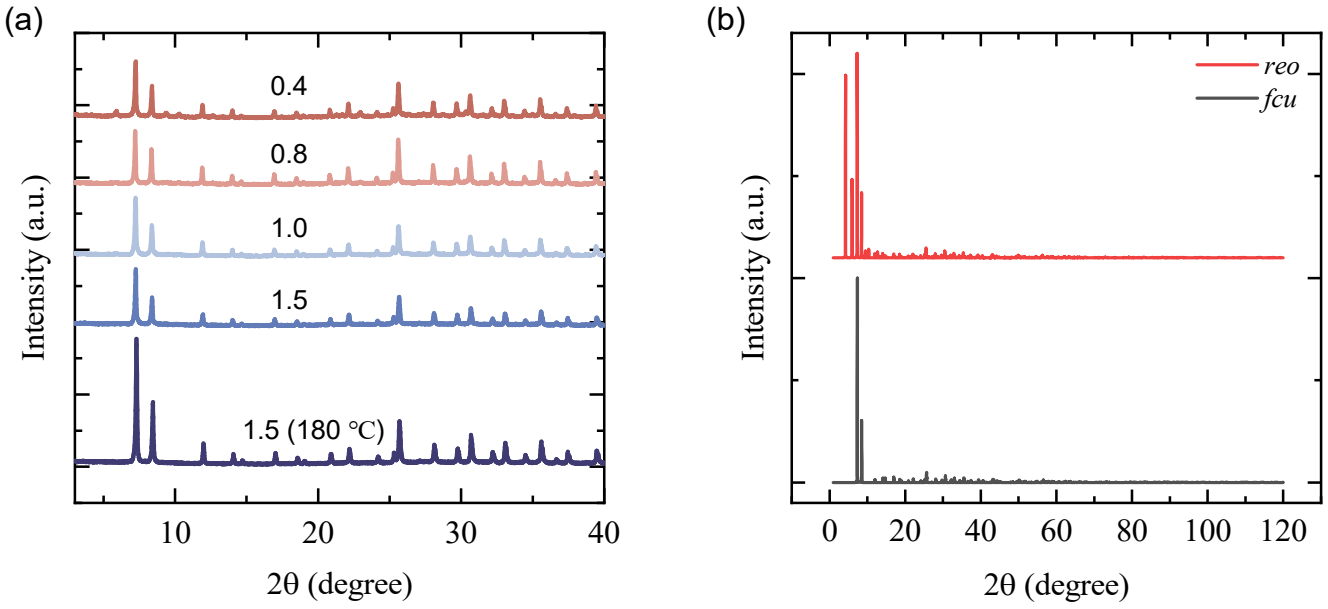

Fig. S1. (a) The PXRD patterns of UiO-66 crystals. (b) The simulated PXRD patterns of UiO-66 with the *fcu* and *reo* topologies.

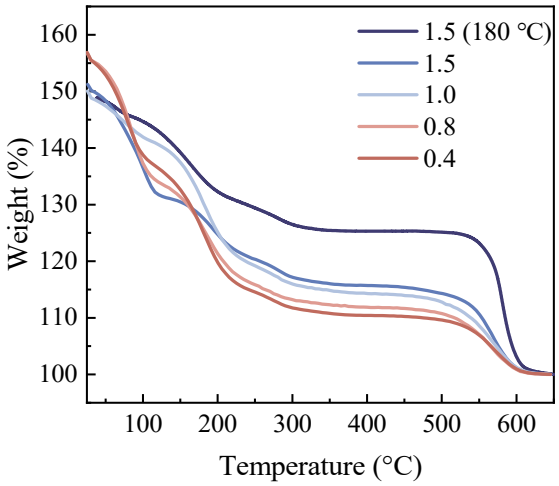

Fig. S2. The TGA patterns of UiO-66 crystals.

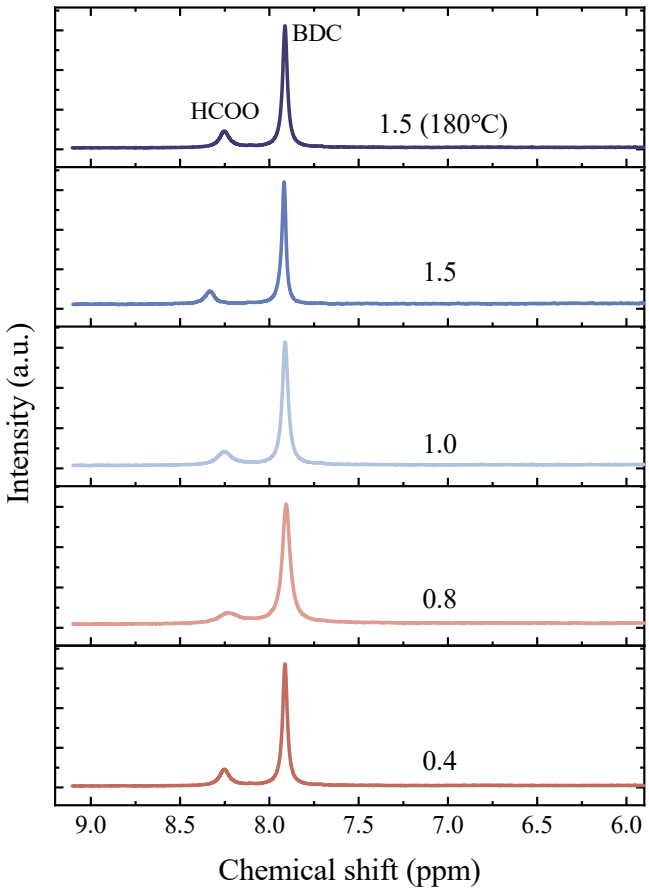

Fig. S3. The ^{1}H-NMR patterns of UiO-66 crystals.

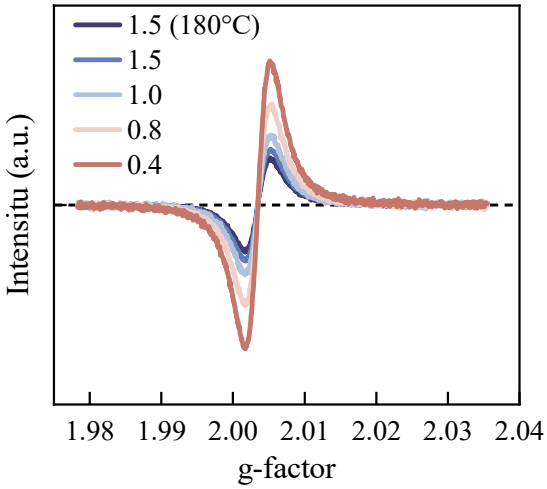

Fig. S4. The EPR diagram of UiO-66 crystals.

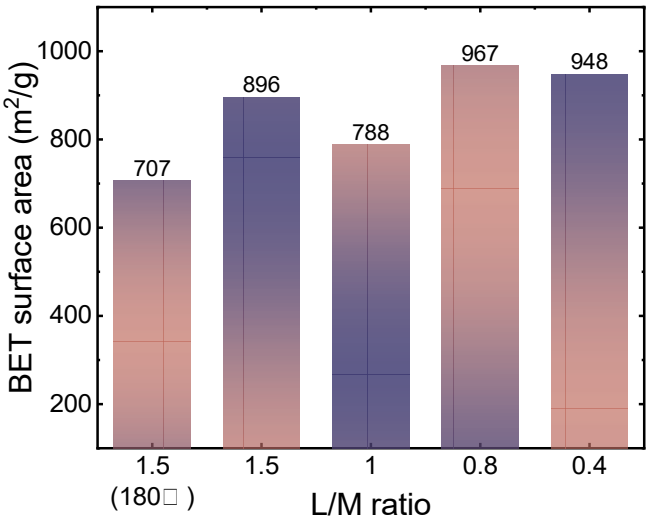

Fig. S5. The BET surface areas of UiO-66 crystals.

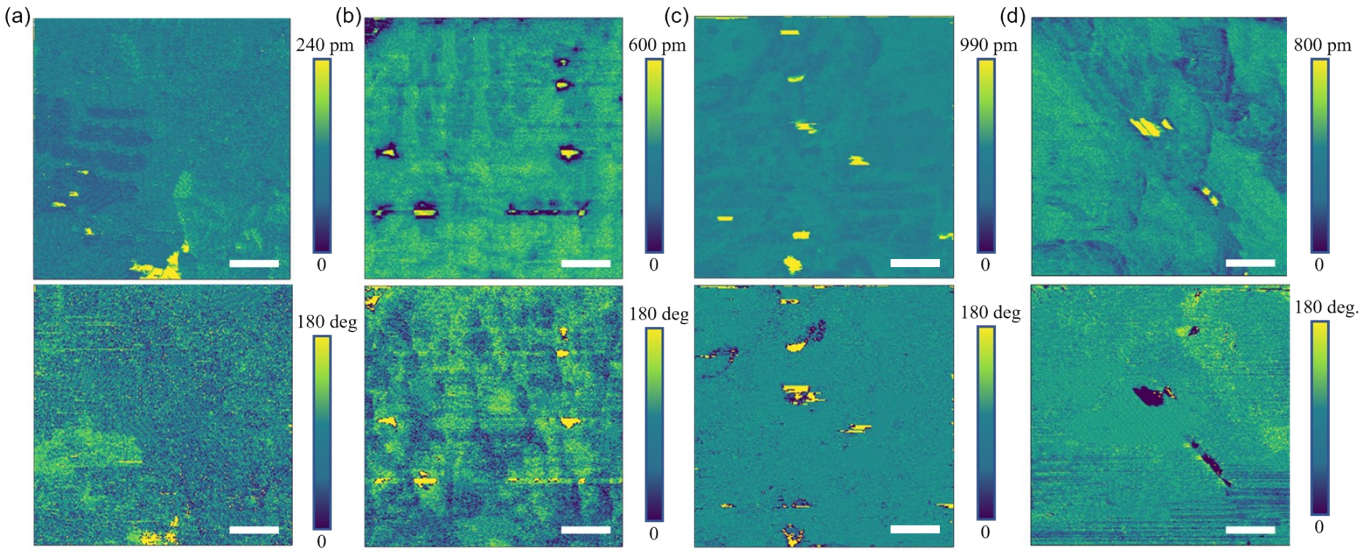

Fig. S6. Piezoelectric amplitudes (top panel) and corresponding phase maps (bottom panel) of UiO-66 with (a) L/M=1.5, (b) L/M=1.0 (c) L/M=0.8 and (d) L/M=0.4. All scale bars are 1 μm.

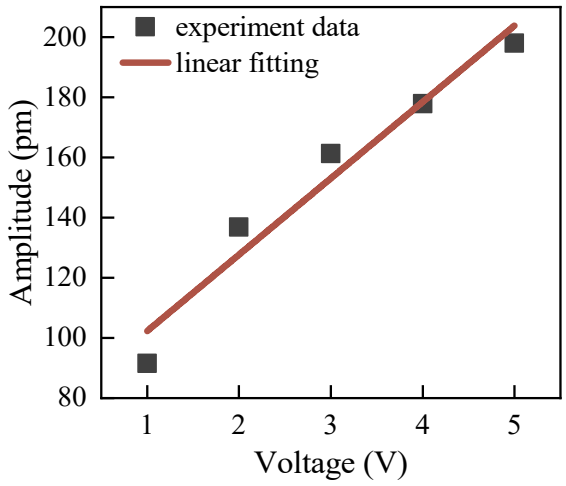

Fig. S7. PFM measurement of the variation of amplitude with applied alternating current voltage for pristine UiO-66 (L/M=1.5, 180 °C).

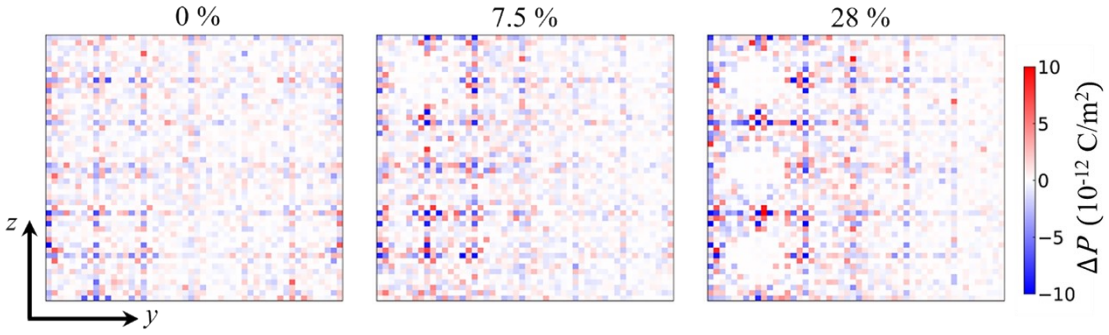

Fig. S8. Distribution of polarization change of pristine UiO-66 and defective UiO-66 with defect concentrations of 7.5% and 28% extracted from MD simulations.

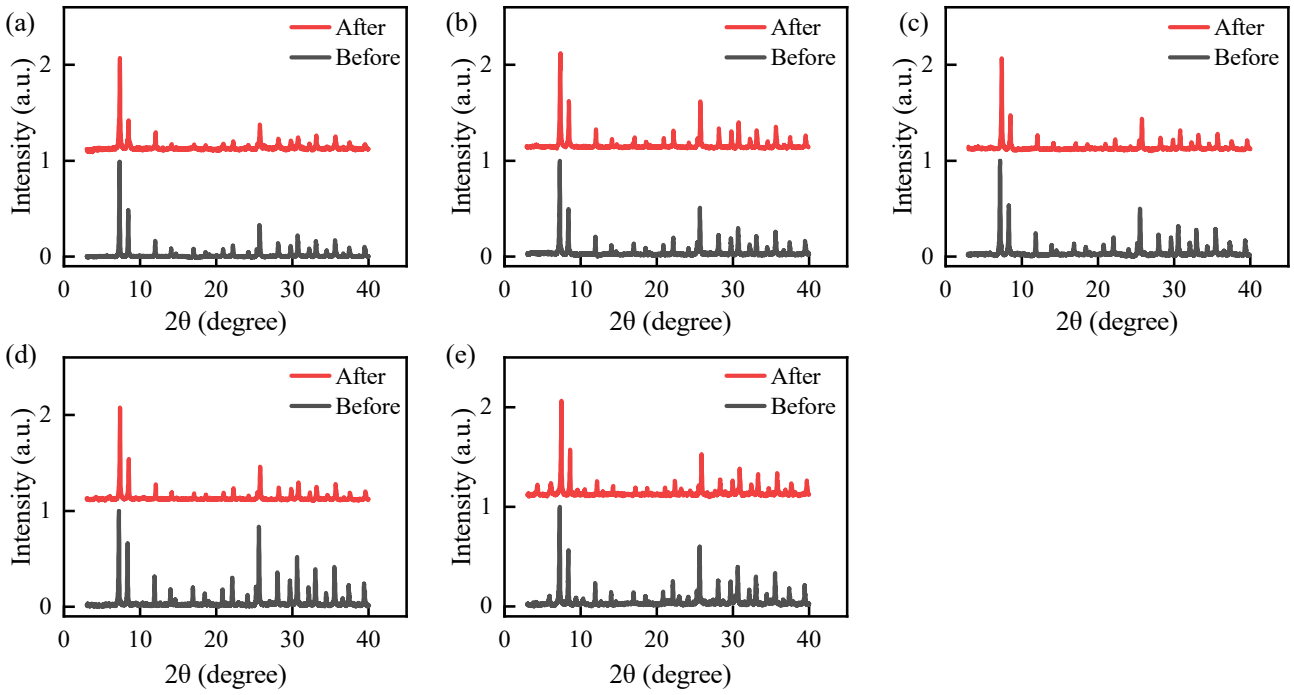

Fig. S9. The PXRD diffraction patterns before ultrasonic vibration and after two hours of ultrasonic vibration for samples with (a) L/M=1.5 (180 °C), (b) L/M=1.5, (c) L/M=1.0 (d) L/M=0.8 and (e) L/M=0.4.

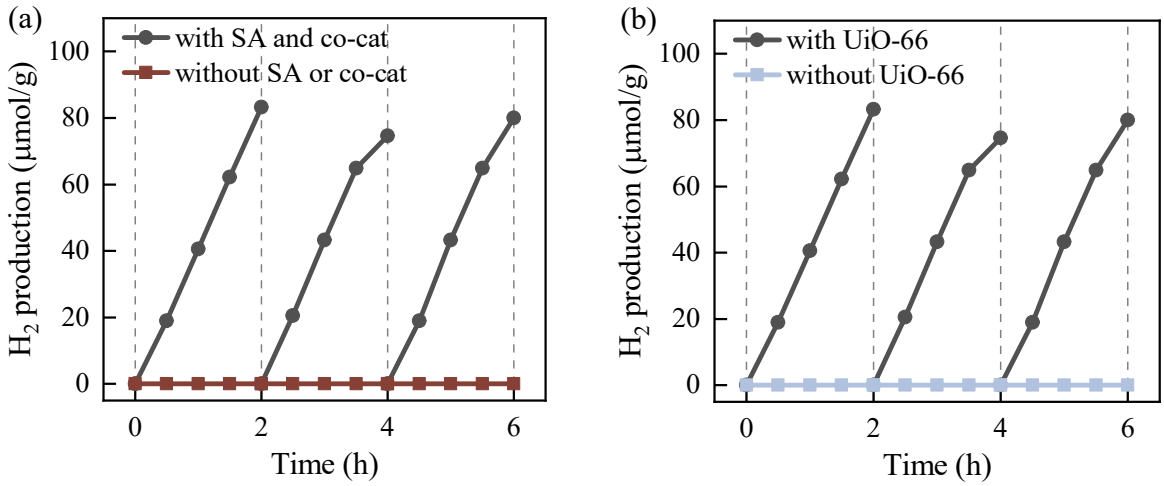

Fig. S10. (a) Hydrogen yields of UiO-66 (L/M = 1.0) under ultrasonic vibration with and without sacrificial agent (SA) and co-catalyst (co-cat). (b) Hydrogen yields in the reaction systems containing H_2O, sacrificial agent (SA), and co-catalyst (co-cat) under conditions with and without UiO-66 (L/M = 1.0).

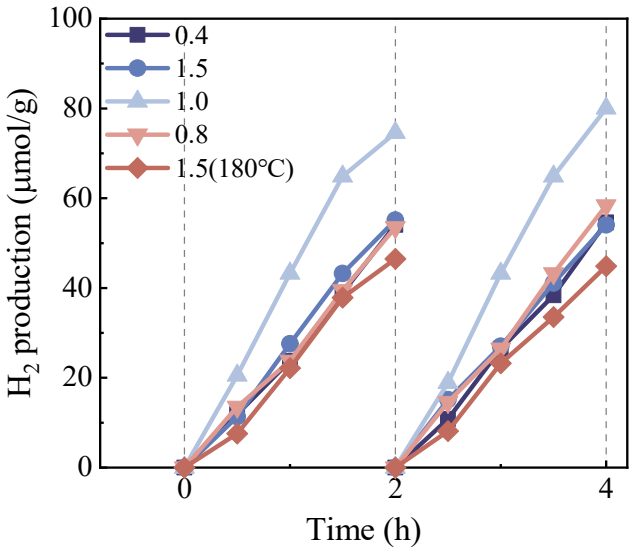

Fig. S11. Two independent replicate tests on hydrogen yields of UiO-66 crystals.

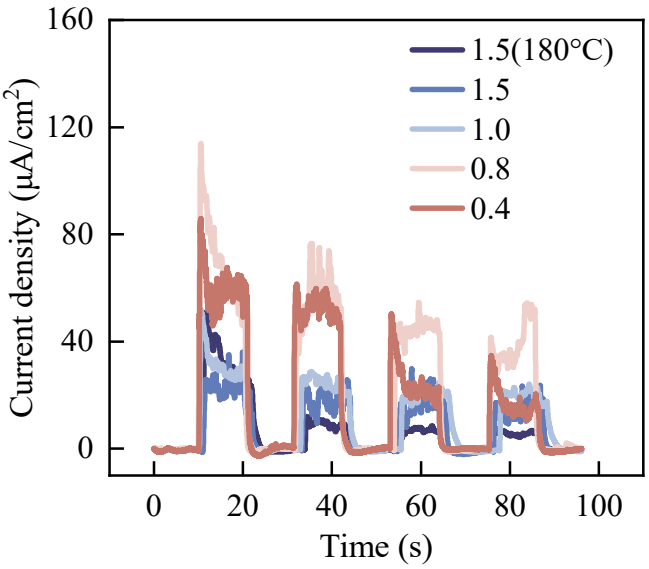

Fig. S12. Transient piezocurrent responses of UiO-66 crystals.

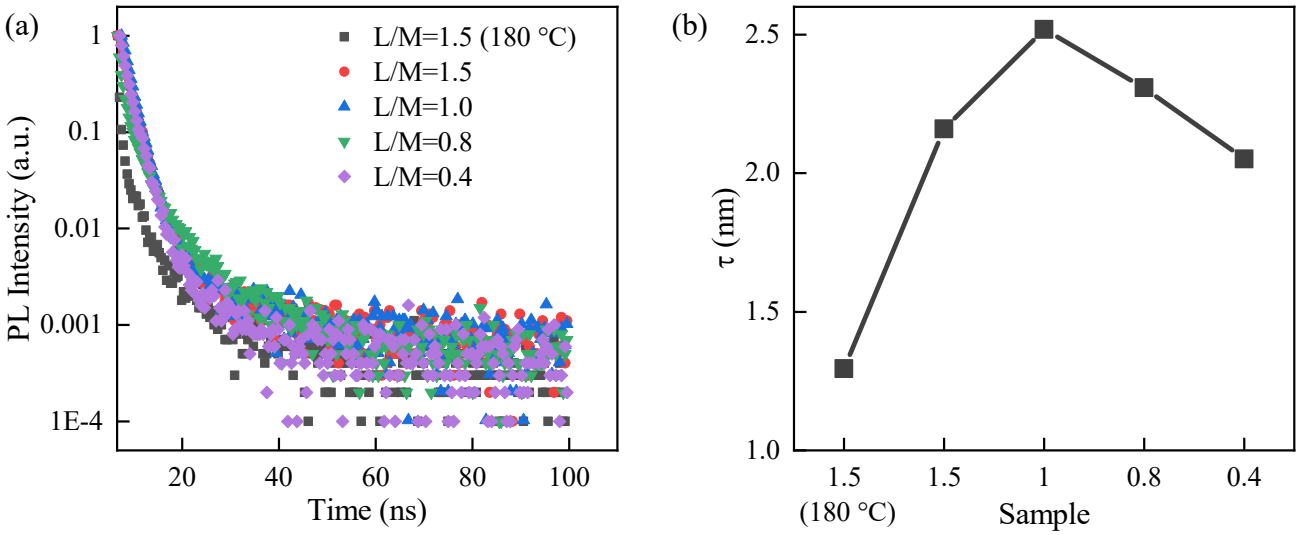

Fig. S13. (a) TRPL decay curves of all synthesized UiO-66 crystals. (b) Average carrier lifetimes (τ) extracted through the bi-exponential fitting of the TRPL curves.

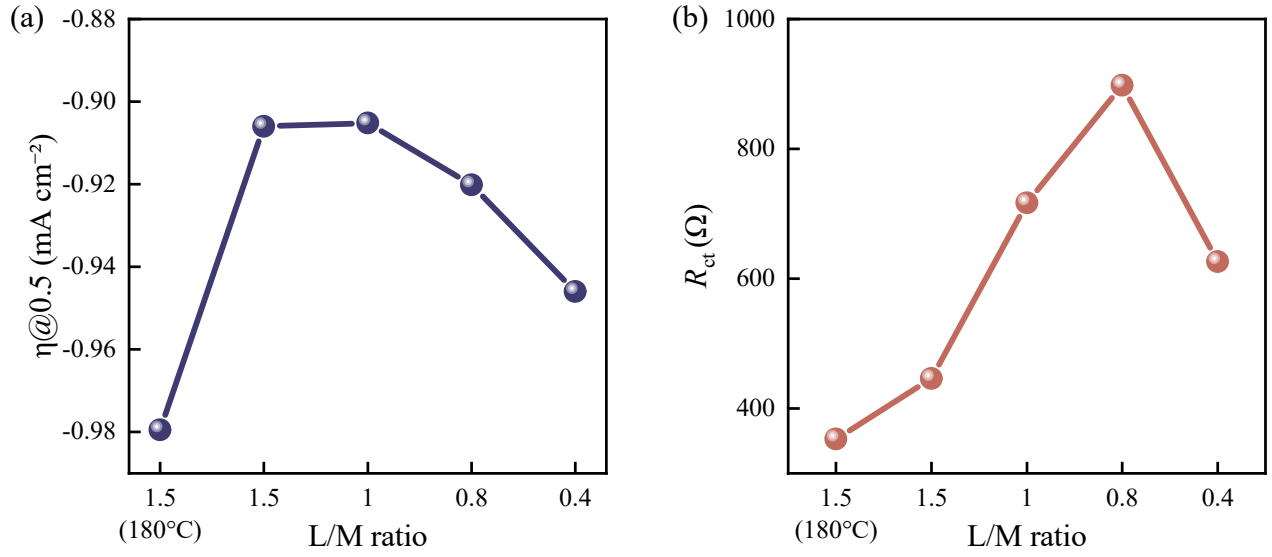

Fig. S14. (a) The overpotential at a fixed current density (η@0.5 mA cm^{-2}) and (b) the charge transfer resistance (R_{ct}) of UiO-66 crystals.

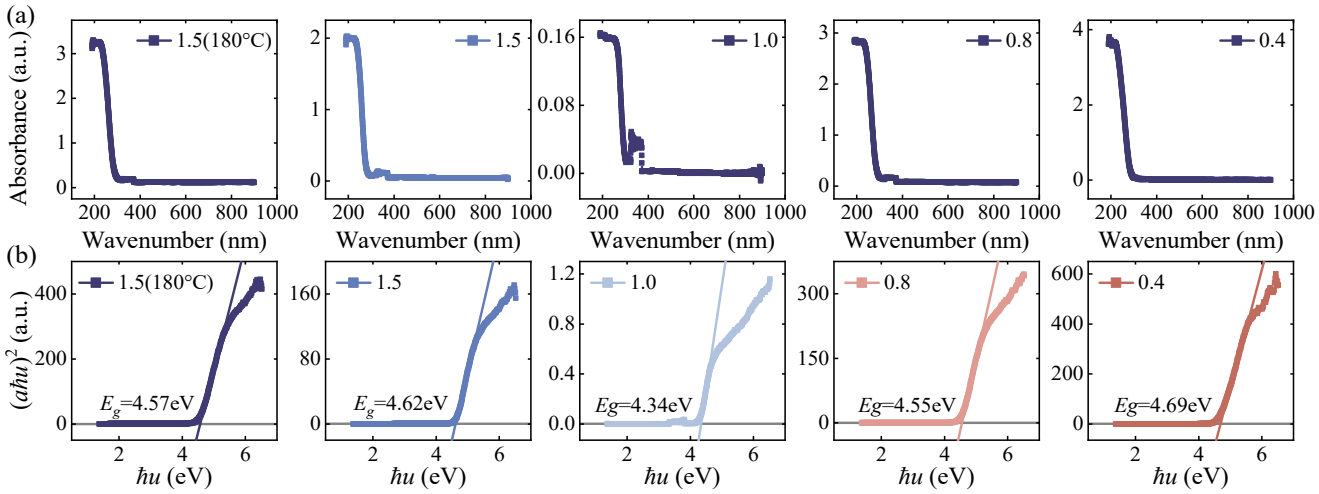

Fig. S15. (a) DR UV-vis spectra and (b) Tauc plots of UiO-66 crystals.

Table S1. Comparative study on hydrogen evolution performance of MOF-based piezocatalysis.

MOF	Conditions	Hydrogen evolution rate	Ref.

		($\mu mol \cdot g^{-1} \cdot h^{-1}$)	
Defective UiO-66(Hf)	220 W, 40 kHz Methanol + $AgNO_3$	UiO-66(L/M=1.5 180 °C): 23.2 UiO-66(L/M=1.0): 39.6	This work
UiO-66(Zr) UiO-66(Zr)-F_4	110 W, 40 kHz Na_2SO_3 + H_2O	UiO-66(Zr): ~0.1 UiO-66(Zr)-F_4: 35.7	S5
Pt/UiO-66-NH_2(Zr)	200 W, 53 kHz	~0.1	S6
Pt/UiO-66-NH_2(Hf)	200 W, 53 kHz	~0.1	S6
NH_2-MIL-125 Cu-NH_2-MIL-125	150 W, 50 kHz Acetonitrile, Water $H_2PtCl_6 \cdot 6H_2O$	MIL-125: ~0.1 NH_2-MIL-125: 5.1 Cu-NH_2-MIL-125: 5.5	S7

Table S2. Position of conduction band (C_B) and position of flat band (V_B) relative to SHE and bandgap (E_g) of UiO-66 crystals.

Sample	C_B (V)	V_B (V)	E_g (eV)
1.5 (180 ℃)	-0.913	3.657	4.57
1.5	-0.773	3.847	4.62
1.0	-1.033	3.307	4.34
0.8	-0.903	3.647	4.55
0.4	-0.803	3.887	4.69

Table S3. Experimental conditions used for pristine and defective UiO-66. The reagents selected were as follows: the metal salt (M) was $HfCl_4$ (Aldrich, 98%), the organic ligand (L) was 1,4-dicarboxylic acid (BDC, Aldrich, 98%), and the modulator (Mod) was formic acid (FA, Alfa Aesar, 97%), N,N-dimethylformamide

(DMF, Scharlau).

Sample	Temperature (℃)	L/M ratio	Mod/L	M (mmol)	L (mmol)	Mod (mmol)	DMF[S8] (mL)	V[S8] (mL)
1.5 (180 ℃)	180	1.5	94.06	0.24	0.36	33.9	4	5
1.5	120	1.5	94.06	0.24	0.36	33.9	4	5
1.0	120	1.0	112,9	0.3	0.3	33.9	4	5
0.8	120	0.8	127.0	0.3	0.3	33.9	4	5
0.4	120	0.4	197.5	0.4	0.2	33.9	4	5

Reference

S1. Tatay, S.; Martinez-Gimenez, S.; Rubio-Gaspar, A.; Gomez-Oliveira, E.; Castells-Gil, J.; Dong, Z.; Mayoral, A.; Almora-Barrios, N.; Padial, N. M.; Marti-Gastaldo, C., Synthetic control of correlated disorder in UiO-66 frameworks. *Nature Communications* **2023,** *14* (1), 6962.

S2. Cliffe, M. J.; Wan, W.; Zou, X.; Chater, P. A.; Kleppe, A. K.; Tucker, M. G.; Wilhelm, H.; Funnell, N. P.; Coudert, F.-X.; Goodwin, A. L., Correlated defect nanoregions in a metal–organic framework. *Nature Communications* **2014,** *5* (1), 4176.

S3. Sivula, K., Mott–Schottky Analysis of Photoelectrodes: Sanity Checks Are Needed. *ACS Energy Letters* **2021,** *6* (7), 2549-2551.

S4. Gelderman, K.; Lee, L.; Donne, S. W., Flat-Band Potential of a Semiconductor: Using the Mott–Schottky Equation. *Journal of Chemical Education* **2007,** *84* (4), 685-688.

S5. Zhao, S.; Liu, M.; Zhang, Y.; Zhao, Z.; Zhang, Q.; Mu, Z.; Long, Y.; Jiang, Y.; Liu, Y.; Zhang, J.; Li, S.; Zhang, X.; Zhang, Z., Harvesting mechanical energy for hydrogen generation by piezoelectric metal–organic frameworks. *Materials Horizons* **2022,** *9* (7), 1978-1983.

S6. Zhang, C.; Lei, D.; Xie, C.; Hang, X.; He, C.; Jiang, H.-L., Piezo-Photocatalysis over Metal–Organic Frameworks: Promoting Photocatalytic Activity by Piezoelectric Effect. *Advanced Materials* **2021,** *33* (51), 2106308.

S7. Hu, H.; Li, X.; Zhang, K.; Yan, G.; Kong, W.; Qin, A.; Ma, Y.; Li, A.; Wang, K.; Huang, H.; Sun, X.; Ma, T., Dual Modification of Metal–Organic Frameworks for Exceptional High Piezo-Photocatalytic Hydrogen

Production. *Advanced Materials* **2025,** *37* (20), 2419023.

S8. Zhang, Y.; Feng, K.; Song, M.; Xiang, S.; Zhao, Y.; Gong, H.; Ni, F.; Dietrich, F.; Fulanović, L.; Zhuo, F.; Buntkowsky, G.; Frömling, T.; Zhang, D.; Bowen, C.; Rödel, J., Dislocation-engineered piezocatalytic water splitting in single-crystal $BaTiO_3$. *Energy & Environmental Science* **2025,** *18* (2), 602-612.